massachusetts institute of technology — artificial intelligence laboratory

Context-Based Vision System for Place and Object Recognition

Antonio Torralba, Kevin P. Murphy, William T. Freeman and Mark A. Rubin

AI Memo 2003-005 March 2003

Abstract

While navigating in an environment, a vision system has to be able to recognize where it is and what the main objects in the scene are. In this paper we present a context-based vision system for place and object recognition. The goal is to identify familiar locations (e.g., office 610, conference room 941, Main Street), to categorize new environments (office, corridor, street) and to use that information to provide contextual priors for object recognition (e.g., table, chair, car, computer). We present a low-dimensional global image representation that provides relevant information for place recognition and categorization, and how such contextual information introduces strong priors that simplify object recognition. We have trained the system to recognize over 60 locations (indoors and outdoors) and to suggest the presence and locations of more than 20 different object types. The algorithm has been integrated into a mobile system that provides real-time feedback to the user. [1]

[1] This work was sponsored by the Air Force under Air Force Contract F19628-00-C-0002. Opinions, interpretations, conclusions, and recommendations are those of the author and are not necessarily endorsed by the U.S. Government.

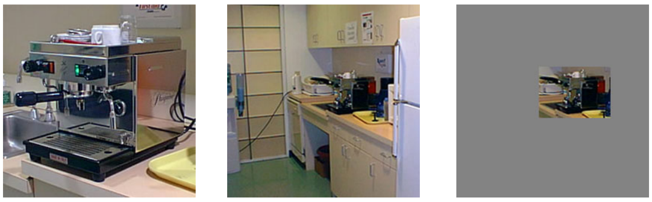

(a) Isolated object (b) Object in context (c) Low-res Object

Figure 1: (a) A close-up of an object; (b) An object in context; (c) A low-res object out of context. Observers in our lab, addicts to coffee, have difficulties in recognizing the coffee machine in figure (c), however, they recognize it in figures (a) and (b).

1. Introduction

We want to build a vision system that can tell where it is and what it is looking at as it moves through the world. This problem is very difficult and is largely unsolved. Our approach is to exploit *visual context*, by which we mean a low-dimensional representation of the whole image (the "gist" of the scene) [4]. Such a representation can be easily computed without having to identify specific regions or objects. Having identified the overall type of scene, one can then proceed to identify specific objects within the scene.

The power of, and need for, context is illustrated in Figure 1. In Figure 1(a), we see a close-up view of an object; this is the kind of image commonly studied in the object recognition community. The recognition of the object as a coffee machine relies on knowing detailed local properties (its typical shape, the materials it is made of, etc.). In Figure 1(b), we see a more generic view, where the object occupies a small portion of the image. The recognition now relies on contextual information, such as the fact that we are in a kitchen. Contextual information helps to disambiguate the identity of the object despite the poverty of the local stimulus (Figure 1(c)).

Object recognition in context is based on our knowledge of scenes and how objects are organized. The recognition of the scene as a kitchen reduces the number of objects that need to be considered, which allows us to use simple features for recognition. Furthermore, the recognition of this scene as a particular kitchen (here, the kitchen of our lab) further increases the confidence about the identity of the object.

While there has been much previous work on object recognition in natural environments, such work has focused on specific kinds of objects, such as faces, pedestrians and cars [14, 3, 5]; these approaches have not generalized to the recognition of many different object categories. Also, advances in multi-view, multi-object recognition have typically been restricted to recognizing isolated objects (e.g., [7]). By contrast, we consider the task of recognizing 24 different types of objects in a natural, unconstrained setting.

2. Global and local image features

The regularities of real world scenes suggest that we can define features correlated with scene properties without having to specifying individual objects within a scene, just as we can build face templates without needing to specify facial features. Some scene features, like collections of views [2, 15] or color histograms [9], perform well for recognizing specific places, but they are less able to generalize to new places (we show some evidence for this claim in Section 3.5). We would like to use features that are related to functional constraints, as opposed to accidental (and therefore highly variable) properties of the environment. This suggests examining the textural properties of the image and their spatial layout.

To compute texture features, we use a wavelet image decomposition. Each image location is represented by the output of filters tuned to different orientations and scales. We use a steerable pyramid [8] with 6 orientations and 4 scales applied to the intensity (monochrome) image. The local representation of an image at an instant t is then given by the jet $v_t^L(x) = \{v_{t,k}(x)\}_{k=1,N}$, where $N = 24$ is the number of subbands.

We would like to capture global image properties, while keeping some spatial information. Therefore, we take the mean value of the magnitude of the local features averaged over large spatial regions:

$$m_t(x) = \sum_{x'} |v_t^L(x')| w(x' - x)$$

where $w(x)$ is the averaging window. The resulting representation is downsampled to have a spatial resolution of $M \times M$ pixels (here we use $M = 4$). Thus, m_t has size $M \times M \times N = 384$. We further reduce the dimensionality by projecting m_t onto the first D principal components (PCs) computed using a database of thousands of images collected with our wearable system. The resulting D-dimensional feature vector will be denoted by v_t^G. This representation proves to be rich enough to describe important scene context, yet is of low enough dimensionality to allow for tractable learning and inference.

Figure 2 illustrates the information that is retained using this representation with $D = 80$ PCs. Each example shows one image and an equivalent textured image that shares the same 80 global features. The textured images are generated by coercing noise to have the same features as the original image, while matching the statistics of natural images [6].

3. Place recognition

In this section we describe the context-based place recognition system. We start by describing the set-up used to capture the image sequences used in this paper. Then we study the problem of recognition of familiar places. Finally

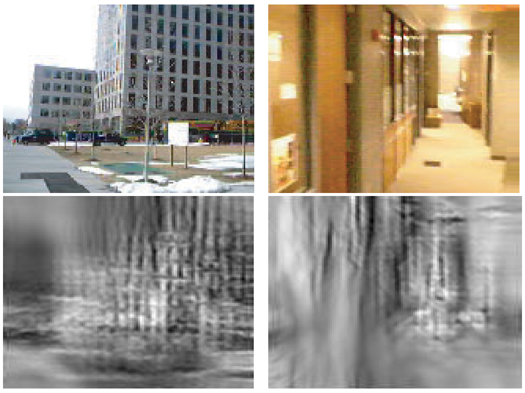

Figure 2: Two images from our data set, and noise patterns which have the same global features. This shows that the features pick up on coarse-grained texture, dominant orientations and spatial organization.

we discuss how to do scene categorization when the system is navigating in a new environment.

3.1 Wearable test bed

As a test-bed for the approach proposed here, we use a helmet-mounted mobile system. The system is composed of a web-cam that is set to capture 4 images/second at a resolution of 120x160 pixels (color). The web-cam is mounted on a helmet in order to follow the head movements while the user explores their environment. The user receives feedback about system performance through a head-mounted display.

This system allows us to acquire images under realistic conditions while the user navigates the environment. The resulting sequences contain many low quality images, due to motion blur, saturation or low-contrast (when lighting conditions suddenly change), non-informative views (e.g., a close-up view of a door or wall), unusual camera angles, etc. However, our results show that our system is reasonably robust to all of these difficulties.

Two different users captured the images used for the experiments described in the paper while visiting 63 different locations at different times of day. The locations were visited in a fairly random order.

3.2 Model for place recognition

The goal of the place recognition system is to compute a probability distribution over the possible places given all the (global) features up to time t. Let the place be denoted by $Q_t \in \{1, \dots, N_p\}$, where $N_p = 63$ is the number of places, and let the global features up to time t be denoted by $v^G_{1:t}$. We can use a hidden Markov model (HMM) to recursively compute $P(Q_t|v^G_{1:t})$ as follows:

$$P(Q_t = q|v^G_{1:t}) \quad \propto \quad p(v^G_t|Q_t = q)P(Q_t = q|v^G_{1:t-1})$$

$$= p(v^G_t|Q_t = q) \sum_{q'} A(q', q)P(Q_{t-1} = q'|v^G_{1:t-1})$$

where $A(q', q) = P(Q_t = q|Q_{t-1} = q')$ is the transition matrix and $p(v^G_t|Q_t)$ is the observation likelihood, which we model by a mixture of K spherical Gaussians:

$$\begin{aligned} p(v^G_t|Q_t = q) \quad &= \\ &\sum_{k=1}^{K} P(Z_t = k|Q_t = q)p(v^G_t|Q_t = q, Z_t = k) \\ &\propto \sum_k W(q, k) \exp\left(\frac{-1}{2\sigma_p^2}||v^G_t - \mu^p_{k,q}||^2\right) \end{aligned}$$

where Z_t is the latent indicator variable, specifying which mixture component to use, and $W(q, k)$ is the weight of mixture component k given $Q_t = q$.

Note that this use of HMMs is different from previous approaches in wearable computing such as [9]. In our system, states represent 63 different locations, whereas Starner et al. used a collection of separate left-to-right HMMs to classify approach sequences to one of 14 rooms. In fact, the model we propose for place recognition is more similar to a topological map of the kind used in the mobile robotics community (e.g., [13, 15]). A topological map can be used to specify one's location at a coarse level, as opposed to a metric map, which is often used to localize a robot to an accuracy of centimeters.

3.3 Training for place recognition

For training, we hand-labeled a set of 17 sequences [1] with their corresponding place names. (Each sequence only visited a subset of the 63 places.) We counted the number of times we transitioned from place i to place j, $C(i, j)$; the maximum likelihood estimate of transition matrix A was obtained by simply normalizing each row of the count matrix, C. The resulting structure of A reflects the topology of the environment. However, to prevent us from asserting that a transition is impossible just because it was not present in the (small) training set, we use a uniform Dirichlet prior with equivalent sample size $s = 0.63$. (This can be implemented by adding a matrix of pseudo counts with values s/N_p to the actual counts.) The prior causes the resulting transition matrix to be fully connected, although many transitions have very low probability.

For the observation model, we estimated σ_p and the number of mixture components, K, using cross-validation; we found $\sigma_p = 0.05$ and $K = 100$ to be the best. Maximum

[1] The training data consisted of 5 sequences from outside the MIT AI lab, 3 from floor 6 of building 400, 4 from floor 9 of building 400, and 5 from floor 7 of building 200. The data was collected using the wearable system described in Section 3.1, over the course of several days during different lighting conditions.

likelihood estimates of the mixing matrix, $W(k,q)$, and the means, $\mu^p_{k,q}$, can be computed using EM. However, in this paper, we adopt the simpler strategy of picking a set of $K(q)$ prototypes as the centers, $\mu^p_{k,q}$, and using uniform weights ($W(k,q) = \frac{1}{K(q)}$); the result is essentially a sparse Parzen window density estimator. Currently the prototypes are chosen uniformly from amongst all views associated with each location. We obtain similar results (but with fewer prototypes) using K-means clustering.

3.4 Performance of place recognition

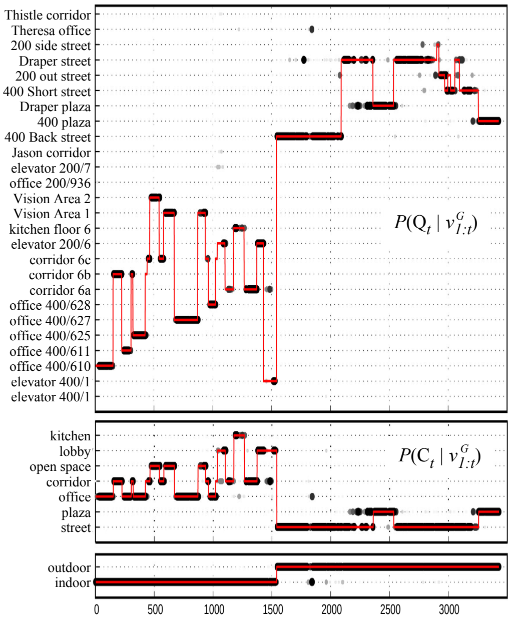

Figure 3: Performance of place recognition for a sequence that starts indoors and then (at frame $t = 1500$) goes outdoors. **Top**. The solid line represents the true location, and the dots represent the posterior probability associated with each location, $P(Q_t|v^G_{1:t})$, where shading intensity is proportional to probability. There are 63 possible locations, but we only show those with non-negligible probability mass. **Middle**. Estimated category of each location, $P(C_t|v^G_{1:t})$. **Bottom**. Estimated probability of being indoors or outdoors.

In this section, we discuss the performance of the place recognition system when tested on a sequence that starts indoors (in building 400) and then (at frame $t = 1500$) moves outdoors. The test sequence was captured in the same way as the training sequences, namely by walking around the environment, in no particular order, but with an attempt to capture a variety of views and objects in each place. A qualitative impression of performance can be seen by looking at Figure 3 (top). This plots the belief state, $P(Q_t|v^G_{1:t})$, over time. We see that the system believes the right thing nearly all of the time. Some of the errors are due the inherent ambiguity of discretizing space into regions. For example, during the interval $t = 2100 : 2200$, the system is not sure whether to classify the location as “Draper street” or “Draper plaza”. Other errors are due to poorly estimating the transition matrix. For example, just before $t = 1500$, there is a transition from “elevator 200/6” to the “floor 1 elevator lobby”, which never occurred in the training set. The Dirichlet prior prevents us from ruling out this possibility, but it is considered unlikely.

In general, the observation likelihood terms, $b_t(q) = p(v^G_t|Q_t = q)$, often dominate the effects of the transition prior. This is a well-known problem with HMMs when using mixtures of high-dimensional Gaussians (see e.g., [1, p142]). We adopt the standard solution of rescaling the likelihood terms; i.e., we use

$$\tilde{b}_t(q) = \frac{p(v^G_t|Q_t = q)^{\gamma_p}}{\sum_{q'} p(v^G_t|Q_t = q')^{\gamma_p}}$$

where the exponent γ_p is set by cross-validation. The net effect is to “balance” the transition prior with the observation likelihoods. (It is possible that a similar effect could be achieved using a density more appropriate to images, such as a mixture of Laplace distributions.)

A more quantitative assessment of performance can be obtained by computing precision-recall curves. The recall rate is the fraction of frames which the system is required to label (with the most likely location); this can be varied by adjusting a threshold, θ, and only labeling frames for which $\max_q P(Q_t = q|v^G_{1:t}) > \theta$. The precision is the fraction of frames that are labeled correctly.

The precision-recall framework can be used to assess performance of a variety of parameters. In Figure 4(a) we compare the performance of three different features, computed by subsampling and then extracting the first 80 principal components from (1) the intensity image, (2) the color image, and (3) the output of the filter bank. We see that the filter bank works the best, then color and finally PCA applied to the raw intensity image.

In Figure 4(b), we show the effect of “turning the HMM off”, by using a uniform transition matrix (i.e., setting $A(i,j) = \frac{1}{N_p}$). It is clear that the HMM provides a significant increase in performance (at negligible computational cost), because it performs temporal integration. We also compared to a simpler approach of averaging $p(v^G_t|Q_t)$ over a temporal window of size W before thresholding as was done in [11]. We found (by cross validation) that $W = 10$ works best, and this is what is shown in Figure 4(b); results for $W = 1$ (i.e., without any temporal averaging) are significantly worse (not shown).

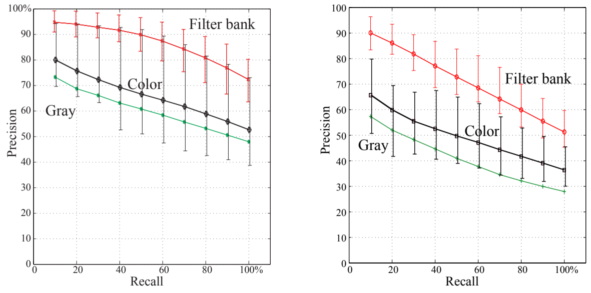

(a) HMM (b) No HMM

Figure 4: Precision-recall curves for different features for place recognition. The solid lines represent median performance computed using leave-one-out cross-validation on all 17 sequences. The error bars represent the 80% probability region around the median. The curves represent different features. From top to bottom: filter bank, color, monochrome (see text for details). **(a)** With HMM ($\gamma_p = 0.2$, $W = 1$, A = learned). **(b)** Without HMM ($\gamma_p = 1$, $W = 10$, A = uniform).

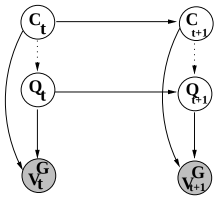

Figure 5: A graphical model for performing simultaneous place recognition and categorization. Q_t (specific place) and C_t (category of place) form part of a taxonomic hierarchy; the indoors/outdoors category level (not shown) could be added on top. The dotted arc from C_t to Q_t is not implemented in this paper.

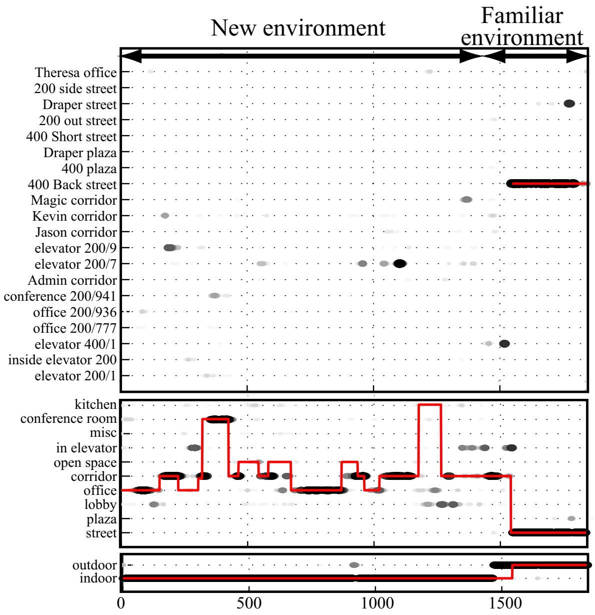

Figure 6: Place categorization when navigating in a new environment not included in the training set (frames 1 to 1500). During the novel sequence, the place recognition system has low confidence everywhere, but the place categorization system is still able to classify offices, corridors and conference rooms. After returning to a known environment (after $t = 1500$), performance returns to the levels shown in Figure 3.

3.5 Scene categorization

In addition to recognizing known places, we would like the system to be able to categorize novel places into various high-level classes such as office, corridor, street, etc. There are several ways to do this. The simplest is to use the HMM described above, and then to sum up the probability mass assigned to all places which belong to the same category. An alternative is to train an HMM on category labels instead of location labels. Finally, we can combine both approaches, as shown in Figure 5. Here $Q_t \in \{1, \ldots, N_p\}$ as before, and $C_t \in \{1, \ldots, N_c\}$, where $N_c = 12$ is the number of categories.

If we assume there is no dependence of locations Q_t on categories C_t, and that the likelihood factorizes as

$$p(v_t^G|Q_t, C_t) = p(v_t^G|Q_t)p(v_t^G|C_t)$$

then the result is equivalent to running two independent HMMs in parallel, which is the approach we adopt in this paper. We should be able to get better performance if we allow the place, Q_t, to depend on the category C_t. Note that $p(v_t^G|Q_t)$ and $p(v_t^G|C_t)$ may have different forms; hence the system can, in principle, learn to use different parts of the v_t^G feature vector for categorization and recognition, a topic we discuss further below.

The model in Figure 5 allows us to estimate the category, $P(C_t|v_{1:t}^G)$, even if we are uncertain about Q_t. We could imagine adding an “unknown place” state to the state-space of Q_t, and automatically learning about new locations. We leave this to future work.

In this paper, we test categorization performance by training a separate HMM on the category labels. We train it on outdoor sequences and indoor sequences from building 200, and then test it on a sequence which starts in building 400 (which it has never seen), and then, at $t = 1500$, moves outside (which it has seen). The results are shown in Figure 6. Before the transition, the place recognition system has a uniform belief state, representing complete uncertainty, but the categorization system performs well. As soon as we move to familiar territory, the place recognition system becomes confident again.

We also computed precision recall curves to assess the performance of different features at the categorization task. The results are shown in Figure 7. Categorization performance is worse than recognition performance, despite the fact that there are fewer states (17 instead of 63). There

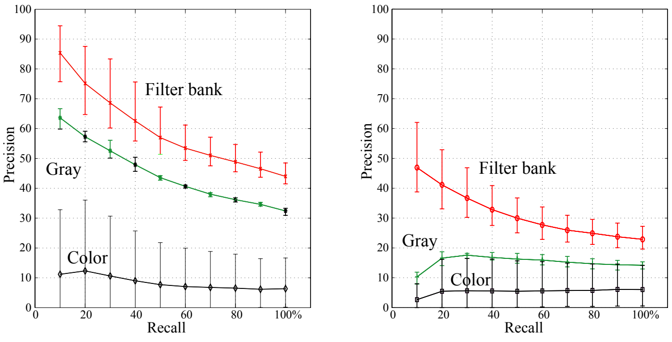

(a) HMM

(b) No HMM

Figure 7: Precision-recall curves for categorization of non-familiar indoor environments. The curves represent different features sets. From top to bottom: filter bank, monochrome and color. Note that now color performs worse than monochrome, the opposite to Figure 4.

are several reasons for this. First, the variability of a class is much larger than the variability of a place, so the problem is intrinsically harder. Second, some categories (such as “open space” and “office”) are visually very similar, and tend to get confused, even by people. Third, we have a smaller training set for estimating $P(C_t|C_{t-1})$, since we observe fewer transitions between categories than between instances.

Interestingly, we see that color performs very poorly at the categorization task. This is due to the fact that the color of many categories of places (such as offices, kitchens, etc.) may change dramatically (see Figure 8) from one environment to the next. The structural composition of the scene, on the other hand, is more invariant. Hence, although color is a good cue for recognition, it is not so good for categorization (with the exception of certain natural “objects”, such as sky, sun, trees, etc.).

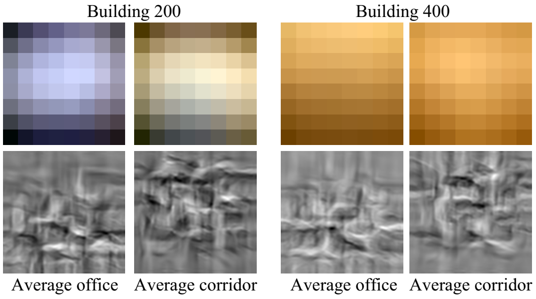

Figure 8: Average of color (top) and texture (bottom) signatures of offices and corridors for two different buildings. This shows that the overall color of offices/corridors varies significantly between the two buildings, whereas the texture features are more stable.

4. From scenes to objects

Most approaches to object detection and recognition involve examining the local visual features at a variety of positions and scales, and comparing the result with the set of all known object types. However, the context can provide a strong prior for which objects are likely to appear, as well as their expected size and position within the image, thus reducing the need for brute force search [12, 10]. In addition, the context can help disambiguate cases where local features are insufficient. In this paper, the context consists of both the global scene representation, v_t^G, and the current location, Q_t. We show how we can use the context to predict properties of objects without even looking at the local visual evidence.

Let $O_{t,i}$ represent the attributes of all objects of type i in image v_t; these could include the number of such objects (zero or more), their size, shape, appearance, etc. Let $\vec{O}_t = (O_{t,1}, \ldots, O_{t,N_o})$, where $N_o = 24$ is the number of object types considered here (bicycles, cars, people, buildings, chairs, computers, etc.). We can compute $P(\vec{O}_t|v_t, Q_t)$ as follows:

$$P(\vec{O}_t|v_{1:t}) \approx \sum_q P(\vec{O}_t|Q_t = q, v_t)P(Q_t = q|v_{1:t})$$

The second term is the output of the HMM, as discussed in Section 3. The first term can be computed using Bayes' rule:

$$\begin{aligned} P(\vec{O}_t|v_t, Q_t) &\propto p(v_t|\vec{O}_t, Q_t)P(\vec{O}_t|Q_t) \\ &\approx \prod_i p(v_t|O_{t,i}, Q_t) \prod_i P(O_{t,i}|Q_t) \end{aligned}$$

where we have assumed that the likelihood of an image factorizes into a product of terms and that objects are a priori conditionally independent (see Figure 9). This allows us to focus on one object (type) at a time.

In order to compute $p(v_t|O_{t,i} = o, Q_t)$, we have to make some approximations. A common approximation is to assume that the object's properties (presence, location, size, appearance, etc.) only influence a set of local features, v_t^o (a subset of v_t). Thus

$$p(v_t|O_{t,i} = o, Q_t = q) = p(v_t^o|o, q)$$

However, the global context is a very powerful cue that we want to exploit. Hence we include some global scene features, v_t^G (a deterministic function of v_t):

$$\begin{aligned} p(v_t|o, q) &= p(v_t, v_t^G|o, q) \\ &= p(v_t|v_t^G o, q)p(v_t^G|o, q) \\ &\approx p(v_t^o|o, q, v_t^G)p(v_t^G|o, q) \end{aligned}$$

The first term, $p(v_t^o|o, q, v_t^G)$, can be approximated by $p(v_t^o|o, q)$ assuming that the object attributes o specify the

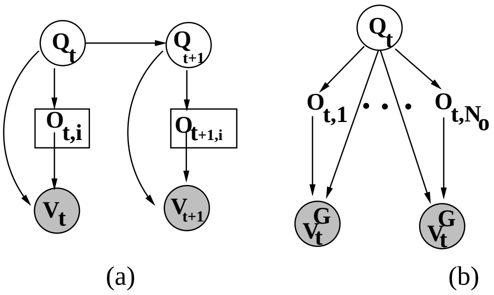

Figure 9: A graphical model illustrating the relationship between the place recognition system (which estimates Q_t), and the object recognition system (which estimates $O_{t,i}$). **a**. The box ("plate") around the $O_{t,i}$ node represents N_o conditionally independent copies of this variable. **b**. The model for a single time slice. This shows that the prior is factored, $P(\vec{O}_t|Q_t) = \prod_i P(O_{t,i}|Q_t)$, and that the likelihood is factored, $p(v_t^G|\vec{O}_t, Q_t) = \prod_i p(v_t^G|O_{t,i}, Q_t)$, which we have indicated graphically by replicating the fixed V_t^G node.

object appearance (although this ignores the effect of some global scene factors, such as lighting). For this paper, we ignore the first term (i.e., $p(v_t^o|o, q, v_t^G)$), and focus on the second term, $p(v_t^G|o, q)$, which is related to the global context.

Putting it all together, we see that we can compute the marginal posterior probability of each object type as follows:

$$P(O_{t,i}|v_{1:t}^G) = \sum_q P(O_{t,i}|v_t^G, Q_t = q)P(Q_t = q|v_{1:t}^G)$$

where $P(Q_t|v_{1:t}^G)$ is the output of the HMM and

$$P(O_{t,i}|v_t^G, Q_t) \propto p(v_t^G|O_{i,i}, Q_t)P(O_{t,i}|Q_t)$$

is the output of the object systems to be discussed below.

4.1 Contextual priming for object detection

In this section, we assume $O_{t,i}$ is just a binary random variable, representing whether any object of type i is present in the image or not. $P(O_{t,i} = 1|v_{1:t}^G)$ can be used to do object priming. We can compute the conditional posterior as follows:

$$P(O_{t,i} = 1|v_t^G, Q_t = q) = \frac{p(v_t^G|O_{t,i} = 1, j)F_i(q)}{p(v_t^G|O_{t,i} = 1, q)F_i(q) + p(v_t^G|O_{t,i} = 0, q)(1 - F_i(q))}$$

where $F_i(q) = P(O_{t,i} = 1|Q_t = q)$ is the probability of finding object i in place q (and hence $1 - F_i(q) = P(O_{t,i} = 0|Q_t = q)$).

We labeled a set of about 1000 images to specify whether or not each type of object was present. ¿From this data set, we estimated F_i for each object type i using a method that is analogous to that used for estimating the HMM transition matrix (see Section 3.3).

We model the conditional likelihood using another mixture of spherical Gaussians:

$$p(v_t^G|O_{t,i} = 1, Q_t = q) \propto \sum_{k=1}^{K(i,q)} \frac{1}{K(i,q)} \exp\left(\frac{-1}{2\sigma_o^2}||v_t^G - \mu_{k,i,q}^o||^2\right)$$

This can be estimated from labeled data in the same way as $p(v_t^G|Q_t)$ was estimated in Section 3.3. We estimate $p(v_t^G|O_{t,i} = 0, Q_t = q)$ similarly, using as prototypes images from location q in which object i was absent.

Figure 10 shows the results of applying this procedure to the same test sequence as used in Section 3.4. The system is able to correctly predict the presence of 24 different kinds of objects quite accurately, without even looking at the local image features. Many of the errors are "inherited" from the place recognition system. For example, just before $t = 1500$, the system believes it is in corridor 6a, and predicts objects such as desks and printers (which are visible in 6a); however, the system is actually in the floor 1 elevator lobby, where the only identifiable object is a red couch.

A more quantitative assessment of performance is provided in Figure 11, where we plot ROC (receiver operating characteristic) curves for 20 of the most frequent object classes. (This can be computed by varying a threshold θ and declaring an object to be present if $P(O_{t,i} = 1|v_{1:t}^G) > \theta$; we then count compare the number of estimated positive frames with the true number. We did this for the same indoor-outdoor sequence as used in Figures 3 and 6.) The easiest objects to detect are things like buildings, which are almost always present in every outdoor scene (in this data set at least). The hardest objects are moving ones such as people and cars, since they are only present in a given context for a small fraction of the time.

4.2 Contextual priors for object localization

In this section, we try to predict the location of an object. We represent the location using an 8×10 bit mask: $M_{t,i,l} = 1$ iff any object of type i overlaps image region l, where $l \in \{1, \ldots, 80\}$. This provides a crude way of representing size/shape, as well as a way of representing multiple objects and multi-modal distributions.

Let $M_{t,i}$ be the whole image mask (an 80-dimensional bit vector). Since $P(M_{t,i,l} = 1) = E[M_{t,i,l}]$, we can summarize the distribution in terms of its marginals using the

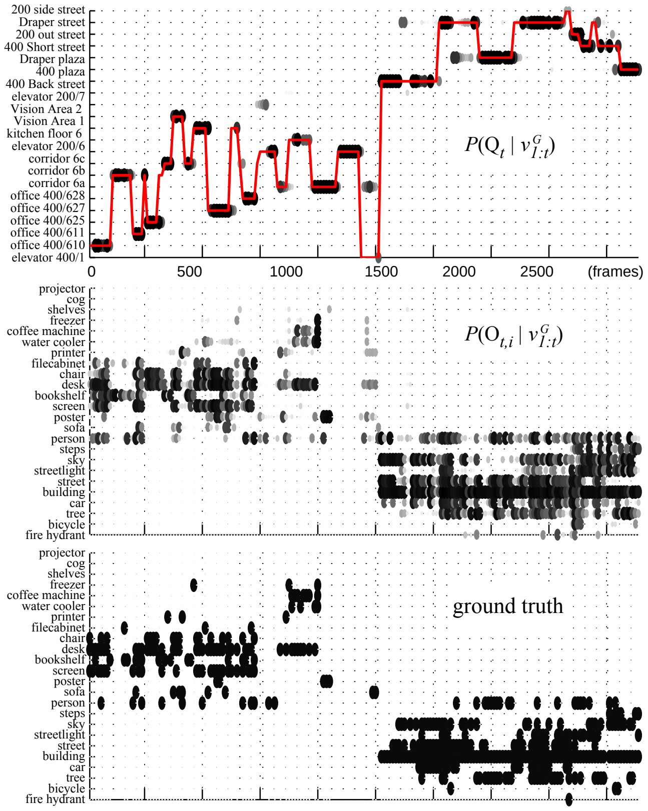

Figure 10: Contextual priors for object detection. We have trained the system to predict the presence of 24 objects. **Top**. The predicted place, $P(Q_t|v^G_{1:t})$ (the same as Figure 3). **Middle**. The probability of each object being present, $P(O_{t,i} = 1|v^G_{1:t})$. **Bottom**. Ground truth: a black dot means the object was present in the image. We only show results for the frames that have ground truth.

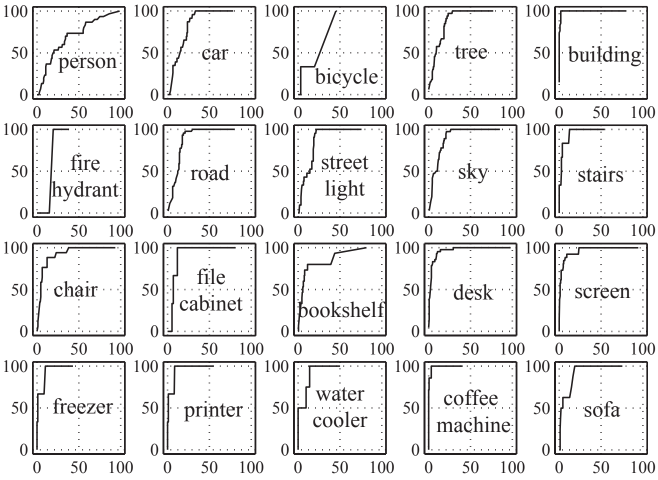

Figure 11: ROC curves for the prediction of object presence in the image. We plot hit rate vs false alarm rate as we vary the threshold on $P(O_{t,i} = 1|v^G_{1:t})$.

expected mask. This can be computed as follows:

$$\begin{aligned} E[M_{t,i}|v^G_{1:t}] &= \sum_{o\in\{0,1\}} \sum_q P(O_{t,i} = o, Q_t = q|v^G_{1:t}) \\ &\quad \times E[M_{t,i}|v^G_t, Q_t = q, O_{t,i} = o] \end{aligned}$$

where $P(O_{t,i}, Q_t|v^G_{1:t})$ was computed by the object priming system discussed in Section 4.1. When the object is absent ($O_{t,i} = 0$), we have $E[M_{t,i}|v^G_t, Q_t, O_{t,i} = 0] = \vec{0}$. If the object is present ($O_{t,i} = 1$), the expected mask is given by

$$E[M_{t,i} = \vec{m}|v^G_t, Q_t, O_{t,i} = 1] = \\ \sum_{\vec{m}} \vec{m} \frac{p(\vec{m}, v^G_t|Q_t, O_{t,i} = 1)}{p(v^G_t|Q_t, O_{t,i} = 1)}$$

We again adopt a kernel density estimator to model the joint on V^G_t and $M_{t,i}$:

$$p(\vec{m}, v^G_t|Q_t = q, O_{t,i} = 1) = \\ \sum_k \frac{1}{K(i,q)} K(\vec{m} - \mu^m_{k,i,q}) K(v^G_t - \mu^o_{k,i,q})$$

where [2] $K(\vec{m} - \mu^m_{k,i,q}) = \delta(\vec{m}, \mu^m_{k,i,q})$ and $K(v^G_t - \mu^o_{k,i,q})$ is the same Gaussian kernel as used in the object priming system. Since the mask kernel is a delta function:

$$\sum_{\vec{m}} \vec{m} \;\; p(\vec{m}, v^G_t|Q_t = q, O_{t,i} = 1) = \\ \sum_k \frac{1}{K(i,q)} \mu^m_{k,i,q} K(v^G_t - \mu^o_{k,i,q})$$

Putting it all together, we get the intuitive result that the expected mask is a set of weighted prototypes, $\mu^m_{k,i,q}$,

$$E[M_{t,i}|v^G_t, Q_t = q, O_{t,i} = 1] = \sum_k w_{k,i,q} \times \mu^m_{k,i,q}$$

$$E[M_{t,i}|v^G_t] = \sum_q \sum_k w_{k,i,q} \times \mu^m_{k,i,q}$$

where the weights are given by how similar the image is to previous ones associated with this place and object combination:

$$w_{k,i,q} = \frac{K_{\sigma_o}(v^G_t - \mu^o_{k,i,q}) \times P(Q_t = q, O_{t,i} = 1|v^G_{1:t})}{\sum_{k'} K_{\sigma_o}(v^G_t - \mu^o_{k',i,q})}$$

where σ_m is the bandwidth (variance) of the Gaussian kernel on views.

[2] We can use kernels with better generalization properties than a delta function. This can be done, for instance, by using other representations for $\vec{m}$ instead of a bit mask. We can model the distribution of masks as $p(\vec{m}) = p(f(\vec{m}))$ where f is a one-to-one mapping. For instance, f can be the function that converts a binary number to an integer. Then, we can use a gaussian kernel $G(f(\vec{m}) - f(\mu^m_{k,i,q}))$.

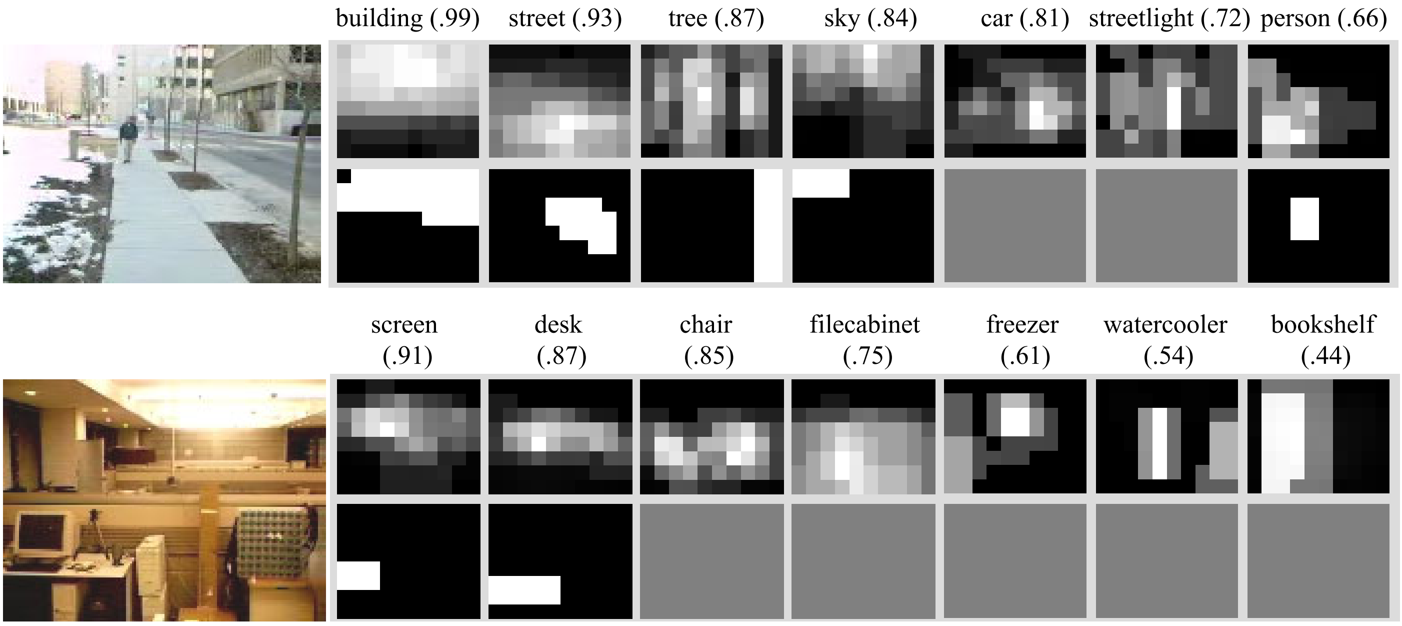

Figure 12: Some results of object localization. The gray-level images represent the probability of the objects being present at that location; the black-and-white images represent the ground truth segmentation (gray indicates absent object). Images are ordered according to $P(O_{t,i}|v^G_{1:t})$.

We trained this model as follows. We manually created a set of about 1000 image masks by drawing polygons around the objects in each image. (The images were selected from the same training set as used in the previous sections.) We then randomly picked up to 20 prototypes $\mu^m_{k,i,q}$ for each location q and object i. A small testing set was created in the same way.

Some preliminary results are shown in Figure 12. The figure shows the probability of each object type appearing in each grid cell (the expected mask $E[M_{t,i}|v^G_{1:t}]$), along with the ground truth segmentation. In some cases, the corresponding ground truth image is blank (gray), indicating that this object does not appear, even though the system predicts that it might appear. Such false positives could be easily eliminated by checking the local features at that position. Overall, we find the results encouraging, despite the small nature of the training set.

Figure 13 shows a summary of the system.

5. Summary and Conclusions

We have shown how to exploit visual context to perform robust place recognition, categorization of novel places, and object priming. Contextual information provides a shortcut for object detection by cutting down the number of possible objects to be considered. In the future, we plan to combine our prior with simple local features, to develop a complete mobile object recognition system.

Acknowledgments

We thank Egon Pasztor (MERL) for implementing the image annotation tool. And also would like to thank Aude Oliva (MSU) for discussions.

References

[1] Y. Bengio. Markovian models for sequential data. *Neural Computing Surveys*, 2:129–162, 1999.

[2] M. O. Franz, B. Scholkopf, H. A. Mallot, and H. H. Bulthoff. Where did i take that snapshot? scene-based homing by image matching. *Biological Cybernetics*, 79:191–202, 1998.

[3] B. Moghaddam and A. Pentland. Probabilistic visual learning for object representation. *IEEE Trans. on Pattern Analysis and Machine Intelligence*, 19(7):696–710, 1997.

[4] A. Oliva and A. Torralba. Modeling the shape of the scene: a holistic representation of the spatial envelope. *Intl. J. Computer Vision*, 42(3):145–175, 2001.

[5] C. Papageorgiou and T. Poggio. A trainable system for object detection. *Intl. J. Computer Vision*, 38(1):15–33, 2000.

[6] J. Portilla and E. P. Simoncelli. A parametric texture model based on joint statistics of complex wavelets coefficients. *Intl. J of Computer Vision*, 40:49–71, 2000.

[7] Bernt Schiele and James L. Crowley. Recognition without correspondence using multidimensional receptive field histograms. *Intl. J. Computer Vision*, 36(1):31–50, 2000.

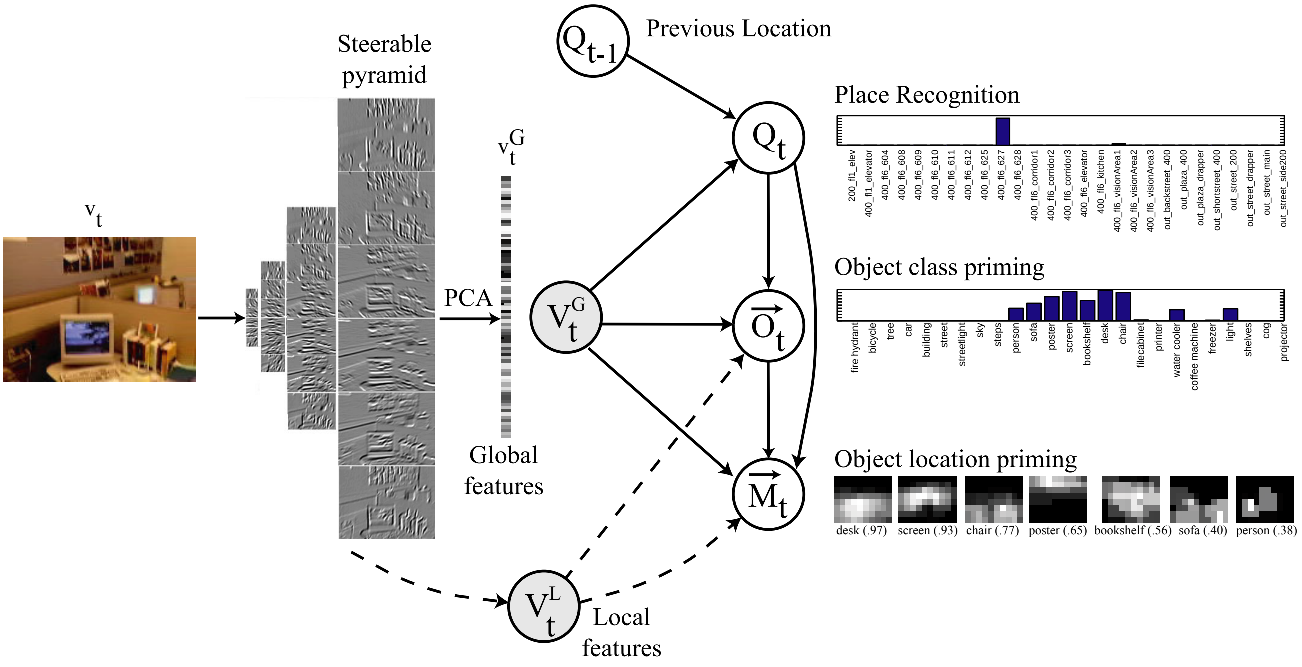

Figure 13: Summary of the context-based system. The dotted lines show how local features could be included in the model. This part is not implemented in the system presented here.

[8] E. P. Simoncelli and W. T. Freeman. The steerable pyramid: A flexible architecture for multi-scale derivative computation. In *2nd IEEE Intl. Conf. on Image Processing*, 1995.

[9] Thad Starner, Bernt Schiele, and Alex Pentland. Visual contextual awareness in wearable computing. In *Intl. Symposium on Wearable Computing*, pages 50–57, 1998.

[10] T. M. Strat and M. A. Fischler. Context-based vision: recognizing objects using information from both 2-D and 3-D imagery. *IEEE Trans. on Pattern Analysis and Machine Intelligence*, 13(10):1050–1065, 1991.

[11] A. Torralba and P. Sinha. Recognizing indoor scenes. Technical report, MIT AI lab, 2001.

[12] A. Torralba and P. Sinha. Statistical context priming for object detection. In *IEEE Conf. on Computer Vision and Pattern Recognition*, pages 763–770, 2001.

[13] I. Ulrich and I. Nourbakhsh. Appearance-based place recognition for topological localization. In *IEEE Intl. Conf. on Robotics and Automation*, 2000.

[14] Paul Viola and Michael Jones. Robust real-time object detection. *Intl. J. Computer Vision*, 2002.

[15] J. Wolf, W. Burgard, and H. Burkhardt. Robust vision-based localization for mobile robots using an image retrieval system based on invariant features. In *Proc. of the IEEE International Conference on Robotics & Automation (ICRA)*, 2002.